Hydrothermal Synthesis, Characterization, and Ionic Conductivity of Vanadium-Stabilized $Bi_{17}V_3O_{33}$ with Fluorite-Related Superlattice Structure

Guangsheng Pang, Shouhua Feng,* Yongchun Tang, Chiheng Tan, and Ruren Xu

Key Laboratory of Inorganic Synthesis and Preparative Chemistry, Department of Chemistry, Jilin University, Changchun 130023, P. R. China

Received March 4, 1998. Revised Manuscript Received June 9, 1998

A novel fluorite-related superlattice structure compound $Bi_{17}V_3O_{33}$ has been synthesized by a hydrothermal method. The content of vanadium and the base concentration in the reaction systems play important roles in the formation of the product. $Bi_{17}V_3O_{33}$ crystallizes in the tetragonal system with cell parameters $a = 1.227(6)$ and $c = 1.104(7)$ nm. Its structure is consistent with a $\sqrt{5} \times \sqrt{5} \times 2$ superlattice based on a fluorite subcell. $Bi_{17}V_3O_{33}$ shows a structural transformation at 802 °C, and the transformed phase, which keeps the main framework structure, is stable until melting at 910 °C. The conductivity of $Bi_{17}V_3O_{33}$ and the transformed phase are 2.14×10^{-4} and 1.03×10^{-3} S·cm^{-1} at 500 °C, respectively.

Introduction

The structures of Bi predominantly containing oxides are usually described as superlattice forms derived from the sublattices of pure Bi_2O_3.[1−5] There are four phases for pure Bi_2O_3, i.e., α, β, γ, and δ forms. α-Bi_2O_3, having a monoclinic structure, is a thermodynamically stable phase below 730 °C. Above 730 °C, the α form transforms to the δ form with a fcc fluorite structure. As temperature decreases further, the δ form transforms to a metastable phase, a tetragonal β form at ca. 650 °C, or a bcc γ form at ca. 639 °C, depending on the quenching conditions.[6−9] Bi-containing oxides have been widely studied for the reason that some of them exhibit high oxide ionic conductivity at temperatures below 800 °C.[10−14] Among them, δ-Bi_2O_3 is the best oxide ion conductor (ca. 1 S·cm^{-1} at 750 °C) known so far.[12,15] δ-Bi_2O_3 contains intrinsic anion vacancies in its fluorite structure, which can be described as $BiO_{1.5}\square_{0.5}$ ($\square$ = vacancy). The structure of the pure δ-Bi_2O_3 phase is not stable at lower temperature, but it can be stabilized by doping with some metal elements, such as V, Nb, Ta, Gd, Mo, W, Y.[13,16] Yttrium in $(Bi_2O_3)_{1-x}(Y_2O_3)_x$ can stabilize the δ-phase down to 25 °C. At 500 °C, a conductivity of the δ-phase with $x = 0.25$ as high as 1.3×10^{-2} S·cm^{-1} has been observed.[17] Studies on the solid-state reaction in Bi_2O_3−V_2O_5 systems claimed that the change of the Bi/V ratio in the starting composition results in a series of compounds, but most of the phases formed are polycrystalline and often occur as intergrowth crystals with closely related structures of comparable or different compositions.[4,5]

Hydrothermal synthesis has been an open route to microporous crystalline and metastable phases, and recently this method has been extended to the preparation of novel and nanocrystalline complex oxides and complex fluorides.[18−20] Compared with conventional solid-state reactions, hydrothermal synthesis is more suitable to obtain metastable and single phases and is favored for homogeneous doping. We extended our study to the Bi−V−O system and obtained a new superlattice phase related to the δ-Bi_2O_3 structure.

Experimental Section

The reactants used in the synthesis were $NaVO_3 \cdot 2H_2O$ (AR grade), $Bi(NO_3)_3 \cdot 5H_2O$ or $BiCl_3$ (AR grade), and NaOH (AR grade). The hydrothermal synthesis of the reaction mixtures with various initial compositions (see Tables 1 and 2) was carried out under autogenous pressure in a Teflon-lined stainless steel autoclave at 180 °C for 5 days. Yellow crystalline powders were obtained. The product was filtered, washed

* To whom correspondence should be addressed.

(1) Zhou, W.; Jefferson, D. A.; Alarion-Franco, M.; Thomas, J. M. *J. Phys. Chem.* **1987**, *91*, 512.
(2) Zhou, W. *J. Solid State Chem.* **1992,** *101,* 1.
(3) Zhou, W.; Jefferson, D. A.; Thomas, J. M. *J. Solid State Chem.* **1987,** *70,* 129.
(4) Zhou, W. *J. Solid State Chem.* **1988,** *76,* 290.
(5) Zhou, W. *J. Solid State Chem.* **1990,** *87,* 44.
(6) Tsubaki, M.; Koto, K. *Mater. Res. Bull.* **1984,** *19,* 1613.
(7) Roth, R. S.; Waring, J. L. *J. Res. Nat. Bur. Stand. Sect. A* **1962,** *66A(6),* 451.
(8) Gattow, G.; Schutze, D. *Z. Anorg. Allg. Chem.* **1964,** 328, 44.
(9) Harwig, H. A. *Z. Anorg. Allg. Chem.* **1978,** *444,* 151.
(10) Kendall, K. R.; Navas, C.; Thomas, J. K.; zur Loye H.-C. *Chem. Mater.* **1996,** *8,* 642.
(11) Takahashi, T.; Esaka, T.; Iwahara, H. *J. Appl. Electrochem.* **1977,** *7,* 303.
(12) Takahashi, T.; Iwahara, H.; Nagai, Y. *J. Appl. Electrochem.* **1972,** *2,* 97.
(13) Takahashi, T.; Iwahara, H. *Mater. Res. Bull.* **1978,** *13,* 1447.
(14) Kudo, T.; Obayashi, H. *J. Electrochem. Soc.* **1976,** *123,* 415.
(15) Harwig, H. A.; Gerards, A. G. *J. Solid State Chem.* **1978,** *26,* 265.
(16) Levin, E. M.; Roth, R. S. *J. Res. Nat. Bur. Stand. Sect. A* **1964,** *68(2),* 197.
(17) Kudo, T.; Obayashi, H. *J. Electrochem. Soc.* **1976,** *123,* 415.
(18) Li, G.; Feng, S.; Li, L. *J. Solid State Chem.* **1996,** *126,* 74.
(19) Zhao, C.; Feng, S.; Chao, Z.; Shi, C.; Xu, R. Ni, J. *J. Chem. Soc., Chem. Commun.* **1996,** 1641.
(20) Pang, G.; Feng, S.; Gao, Z.; Xu, Y.; Zhao, C.; Xu, R. *J. Solid State Chem.* **1997,** *128,* 313.

S0897-4756(98)00128-8 CCC: $15.00
Published on Web 08/15/1998

Table 1. The Starting Reactant Compositions, Reaction Conditions and Product Phases

reactant mole ratio				main product phase[a]
$BiCl_3$	$NaVO_3 \cdot 2H_2O$	NaOH	H_2O	
1	0.33	10.8	300	A
1	0.67	10.8	300	B
1	1	10.8	300	B
1	1.33	10.8	300	B
1	1.67	10.8	300	B,U
1	1	8.1	300	U
1	1	16.2	300	B
1	1	21.6	300	A
1	1	27	300	A
1	1	32.4	300	A

[a] A, γ-Bi_2O_3-like structure phase; B, $Bi_{17}V_3O_{33}$; U, unknown phase.

Table 2. the Starting Reactant Compositions, Reaction Conditions and Product Phases

NaOH (M)	product phases for different $Bi(NO_3)_3 \cdot 5H_2O$:$NaVO_3 \cdot 2H_2O$ mole ratios[a]					
	0.2:0.8	0.3:0.7	0.4:0.6	0.5:0.5	0.6:0.4	0.7:0.3
4.0	B	B	B	B	B	B
3.5	B	B	B	B	B	B
3.0	B	B	B	B	B	B
2.5	B	B	B	B	B	B, U
2.0	B	B, U	B, U	B, U	B, U	U
1.5	U	U	U	U	U	U
1.0	U	U	U	U	U	U

[a] B, $Bi_{17}V_3O_{33}$; U, unknown phase.

with deionized water, and dried in air at ambient temperature. To allow comparison with the results of the solid-state method, a solid-state reaction was performed with a stoichiometric composition of Bi_2O_3 and V_2O_5 at 820 °C for 24 h in air. The contents of Bi and V in the product were determined by ICP-AE spectrometer to be 83.76 wt % Bi and 3.63 wt % V.

Powder X-ray diffraction (XRD) analysis was performed on a Rigaku D/max-γA diffractometer with graphite-filtered CuKα radiation. XRD data were collected over the range 8−70° with a step interval of 0.02° and a preset time of 2 s per step at room temperature. Silicon was used as an external standard and absolute zero error was evaluated as less than 0.01° (2θ). Generator operating conditions were 50 kV and 150 mA; slit, DS/SS 1°, RS/RS_m 0.6/0.6 mm. The precise determination of the peak positions and multipeak and Kα_2 stripping was carried out by using a program available in a software package that does line shape Fourier analysis. The indexing of the XRD pattern and determination of cell parameters were performed by utilizing a computer program, DICVOL91, which is based on the successive dichotomy method and tackles any symmetry.[21]

Selected area electron diffraction (SAED) was performed on JEM-2000EX electron microscope. Differential thermal analysis (DTA) was conducted on a DTA-7000 series thermal analysis instrument in air with a heating rate of 20 °C/min. Raman spectra were recorded on a Bruker RFS 100 in the range 10−1200 cm^{-1} with 2 cm^{-1} resolution.

Ionic conductivity was measured in air by a complex AC impedance method from 300 to 750 °C with a ZL5-type precise LCR bridge equipped with an IBM computer for data collection in a frequency range from 12 Hz to 100 kHz. The sample was cold-pressed into a pellet (14 mm in diameter, 2 mm thick) under a pressure of 1.6×10^2 MPa. The pellet sample was sintered at 700 or 850 °C for 24 h. The faces of the pellet were coated with platinum ink and heated at 650 °C for 30 min to evaporate the solvent. For conductivity measurements, the pellet was sandwiched between two platinum plates. Both cell and furnace were grounded to avoid the generation of a stray ac field.

(21) Boultif, A.; Louer, D. *J. Appl. Crystallogr.* **1991,** *24*, 987.

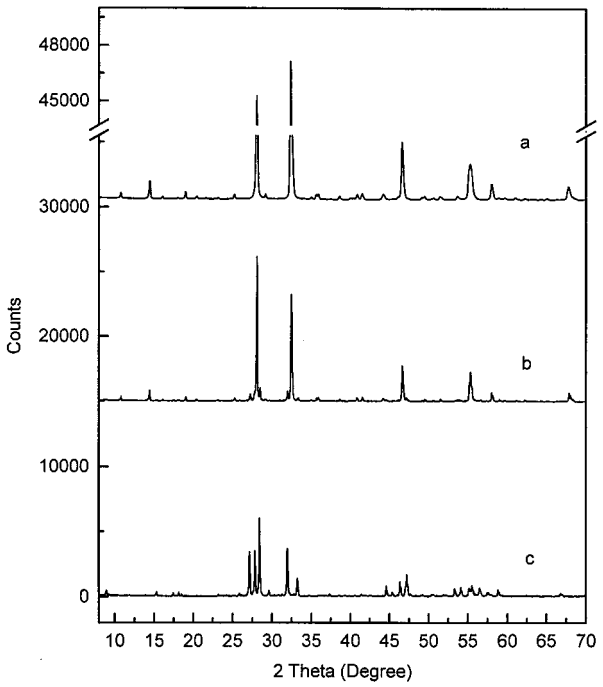

Figure 1. X-ray powder diffraction patterns of (a) $Bi_{17}V_3O_{33}$, (b) the sample after being heated at 850 °C, and (c) the product obtained by solid-state reaction.

Results and Discussion

It was noted that the important factors influencing the formation of $Bi_{17}V_3O_{33}$ are the content of vanadium and the base concentration in the reaction mixtures. The starting reactant compositions, reaction conditions, and product phases are listed in Table 1. In the hydrothermal system, $Bi_{17}V_3O_{33}$ could be obtained from 2−3 M NaOH solution with a Bi/V ratio of 1/1 in reaction mixture. With a lower Bi/V ratio, the γ-Bi_2O_3-like structure phase was obtained, whereas a higher Bi/V ratio led to a phase of unknown structure, which was also obtained by increasing NaOH content to greater than 3 M. When the concentration of NaOH solution was fixed at 2 M, the ratios of Bi/V in a range 3−0.6 were needed for preparing the pure phase of $Bi_{17}V_3O_{33}$.

The bismuth source can be either $BiCl_3$ or $Bi(NO_3)_3 \cdot 5H_2O$. The use of $Bi(NO_3)_3 \cdot 5H_2O$ as bismuth source allowed a wide range of reactant compositions in which the product could be obtained (Table 2). If Bi_2O_3 and V_2O_5 were used as the bismuth and vanadium sources, respectively, $Bi_{17}V_3O_{33}$ mixed with a small amount of γ-Bi_2O_3-like phase was obtained.

It was found that varying the synthesis conditions, such as reactant composition and the base concentration, has no effect on the stoichiometric composition of $Bi_{17}V_3O_{33}$. This is confirmed by composition analysis.

Figure 1a−c shows the XRD patterns of $Bi_{17}V_3O_{33}$, the sample after being heated at 850 °C, and the product obtained by solid-state reaction with $Bi_{17}V_3O_{33}$ of a similar composition. From the XRD patterns, we found that there are significant differences between the structures of $Bi_{17}V_3O_{33}$ and the product obtained by solid-state reaction. The XRD pattern of the product obtained by the solid-state reaction is similar to that of type II phases, as reported by Zhou.[4,5] The XRD pattern of $Bi_{17}V_3O_{33}$ has two main features: (1) the main peaks of $Bi_{17}V_3O_{33}$ are similar to those of δ-Bi_2O_3. This implies

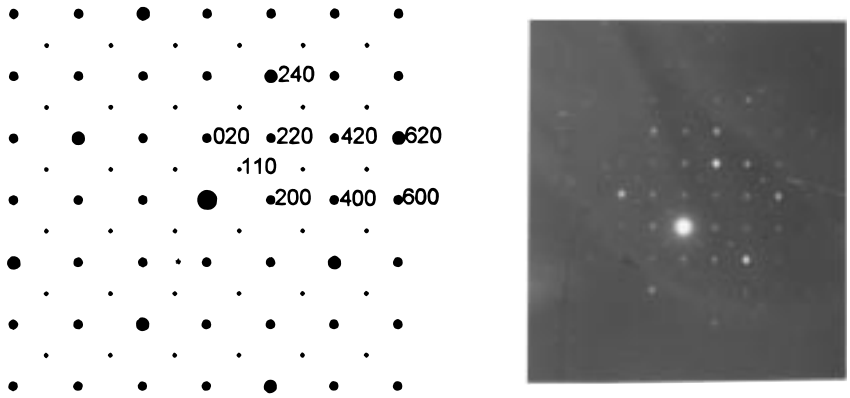

Figure 2. The electron diffraction pattern of $Bi_{17}V_3O_{33}$ in the [001] projection.

Table 3. Powder X-ray Diffraction Data for $Bi_{17}V_3O_{33}$

h	*k*	*l*	D_{OBS}	D_{CAL}	I/I_o	*h*	*k*	*l*	D_{OBS}	D_{CAL}	I/I_o
1	0	1	8.212	8.212	2.5	5	3	2	1.9671	1.9673	1
2	0	0	6.132	6.138	8.1	4	2	4	1.9461	1.9469	26.5
0	0	2	5.518	5.524	<1	5	4	1	1.8889	1.8890	<1
2	1	1	4.917	4.916	<1	3	2	5	1.8538	1.8534	<1
1	1	2	4.661	4.660	3.1	0	0	6	1.8413	1.8412	1.4
2	2	0	4.341	4.340	1	5	4	2	1.8108	1.8112	2
2	0	2	4.106	4.106	<1	1	1	6	1.8014	1.8011	<1
3	0	1	3.833	3.837	<1	4	1	5	1.7741	1.7743	1.3
1	0	3	3.528	3.527	2.1	0	7	1	1.7322	1.7321	<1
3	1	2	3.177	3.176	89	4	4	4	1.7058	1.7064	1.4
2	1	3	3.060	3.058	2.1	3	1	6	1.6637	1.6636	<1
4	0	1	2.957	2.957	<1	7	1	2	1.6560	1.6562	16.5
1	4	1	2.876	2.875	<1	5	5	2			
0	0	4	2.761	2.762	100	7	3	0	1.6120	1.6119	<1
4	0	2	2.682	2.683	<1	6	2	4	1.5880	1.5881	7.1
1	1	4	2.632	2.632	<1	1	4	6	1.5663	1.5660	<1
3	3	2	2.563	2.563	<1	4	4	5	1.5482	1.5482	<1
2	0	4	2.519	2.519	1.9	2	4	6	1.5293	1.5291	<1
3	2	3	2.499	2.500	2.2	2	1	7	1.5170	1.5167	<1
4	2	2	2.458	2.458	<1	6	1	5	1.4899	1.4901	<1
4	3	1	2.398	2.397	<1	3	0	7	1.4721	1.4725	<1
5	0	1				1	5	6	1.4629	1.4625	<1
2	2	4	2.330	2.330	1.3	5	4	5	1.4481	1.4481	<1
3	1	4	2.251	2.250	<1	3	2	7	1.4320	1.4318	<1
5	2	1	2.232	2.233	1.9	7	4	3	1.4072	1.4071	<1
5	1	2	2.206	2.207	2	1	8	3			
1	0	5	2.173	2.174	2.5	4	1	7	1.3942	1.3944	<1
6	0	0	2.047	2.046	2.1	7	5	2	1.3816	1.3817	5.8
						0	7	5	1.3738	1.3736	<1

that the structure of $Bi_{17}V_3O_{33}$ is related to δ-Bi_2O_3. (2) A series of weak peaks due to the superstructure based on a fluorite subcell were found. The XRD pattern of $Bi_{17}V_3O_{33}$ can be indexed in the tetragonal system with cell parameters $a = 1.227(6)$ nm, $c = 1.104(7)$ nm, and $V = 1.664(9)$ nm^3. The indexing results of the XRD study are lists in Table 3.

After being heated at 850 °C, $Bi_{17}V_3O_{33}$ showed a structure change, but the main framework was retained, as the main peaks in its XRD pattern remained unchanged. The DTA for $Bi_{17}V_3O_{33}$ shows a small endothermic peak at 802 °C and a large one at 910 °C. XRD studies for the samples heated at various temperatures indicate that a small structural transformation occurred at 802 °C, and the final phase is stable until melting at 910 °C.

Figure 2 shows the SAED pattern of $Bi_{17}V_3O_{33}$ in the [001] projection. The diffraction spots are indexed in the tetragonal system. The strong diffraction spots, such as 240, 620, correspond to the diffraction of the fluorite subcell lattice, and the medium and weak spots, such as 200, 400, 220, 110, correspond to the diffraction of the superstructure lattice. It is clearly seen that there is a 26.57° rotation between the superlattice of

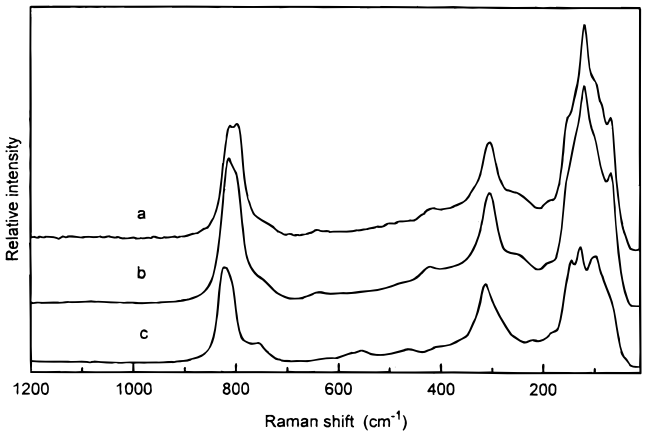

Figure 3. The Raman spectra of (a) $Bi_{17}V_3O_{33}$, (b) the sample after being heated at 850 °C, and (c) the product obtained by solid-state reaction.

$Bi_{17}V_3O_{33}$ and the fluorite sublattice. The result of the SAED is consistent with the indexing result of the XRD study. Compared with theXRD indexing result, the 110 diffraction is too weak to be observed by XRD. Diffraction lines such as those for 200, 020, 220, and 600 appeared in both the XRD and SAED patterns, whereas 240 and 620 diffractions show up as shoulders on the strong diffractions 004 and 424 in the XRD pattern and are difficult to separate.

Taking into account of the cell parameter of δ-Bi_2O_3, 0.5525 nm, the structure of $Bi_{17}V_3O_{33}$ can be described as a $\sqrt{5} \times \sqrt{5} \times 2$ superlattice structure based on a fluorite subcell. The new supercell content has 40 cation sites per unit cell. The elemental analysis results confirmed the formula of the compound as $Bi_{17}V_3O_{33}$. The relationship between the superstructure of $Bi_{17}V_3O_{33}$ and the fluorite subcell can be described as $a_t = a_f + 2b_f$ and $c_t = 2c_f$, where a_t and c_t are the unit cell vectors of superstructure and a_f, b_f, and c_f are the unit cell vectors of the fluorite subcell. The ratio of c_t/a_t is 1.111, which is consistent with the ideal value 1.118. The superstructure of $Bi_{17}V_3O_{33}$ was supported by the SAED results.

To verify the coordination environment of vanadium atoms in the structure, Raman spectroscopy was employed. Figure 3a–c shows the Raman spectra of $Bi_{17}V_3O_{33}$, the sample after being heated at 850 °C, and the product obtained by solid-state reaction. In the Raman spectrum of vanadium–oxide systems, bands at ca. 800 cm^{-1} are usually assigned to the VO_4 tetrahe-

dron vibration.[22] $Bi_{17}V_3O_{33}$ shows two very strong Raman bands at 813 and 796 cm^{-1}, respectively. The intensity of the band at 796 cm^{-1} for the heated sample decreased and a shoulder appeared on the remaining strong band at 813 cm^{-1}. The product obtained by solid-state reaction absorbed very strong and showed medium bands at 823 and 754 cm^{-1}, respectively. According to the Raman results, the VO_4 tetrahedron in $Bi_{17}V_3O_{33}$ is more regular than that in the product obtained by solid-state reaction. Although there are two sorts of V−O bonds, the VO_4 tetrahedron in $Bi_{17}V_3O_{33}$ is nearly perfect, whereas VO_4 in the product obtained by the solid-state reaction is strongly distorted, as there are three short V−O bonds and one long V−O bond.[22] For the high-temperature phase, the intensity of the band at 796 cm^{-1} decreased, showing a structural transformation, as indicated by XRD and DTA. This implies that the VO_4 tetrahedron distorted after the sample was heated to over 802 °C, because the number of long V−O bonds decreased and the number of short V−O bonds increased.

The reason for the formation of a superlattice structure for $Bi_{17}V_3O_{33}$ is the incorporation of vanadium atoms. One vanadium atom is associated with four anion vacancies and occupies a special position in the structure of $Bi_{17}V_3O_{33}$. In the normal fluorite structure, the coordination number of the cation should be 8, but in this case, the V atoms are present as VO_4 tetrahedra, and there are four anion vacancies associated with each vanadium atom in the fluorite structure. If vanadium atoms occupy the positions which are apart from each other, there should be 24 anion vacancies per unit cell, but there are only 14 anion vacancies per unit cell of $Bi_{17}V_3O_{33}$. Therefore, some of the anion vacancies must be shared by vanadium atoms. In considering the relationship of the anion vacancies and the number of vanadium atoms sharing them, i.e., at least six anion vacancies are needed when they are shared by two vanadium atoms, three vanadium atoms correspond to eight anion vacancies, and four vanadium atoms correspond to 10 anion vacancies. Therefore, we conclude that 14 anion vacancies are shared by six vanadium atoms per unit cell and such six vanadium atoms must occupy the central part of the unit cell.

The anion vacancies in $Bi_{17}V_3O_{33}$ imply a considerable anion mobility. On heating $Bi_{17}V_3O_{33}$ at high temperature, the mobility of the anions increases. Although a structural transformation for the superstructure of $Bi_{17}V_3O_{33}$ is observed, the main framework structure for ion motion is kept. The structural transformation can be explained as a result of the distortion of VO_4 in $Bi_{17}V_3O_{33}$. Apparently, $Bi_{17}V_3O_{33}$ is a metastable phase, and this phase shows a temperature dependence and cannot be prepared by a high-temperature solid-state reaction.

Figure 4a,b shows the temperature dependence of conductivity for the samples sintered at 700 and 850 °C, respectively. The relationship between conductivity and the reciprocal of the absolute temperature for both samples is linear over the temperature range measured. The activation energies for ionic conduction for $Bi_{17}V_3O_{33}$ and the heated sample (high-temperature phase after 802 °C) are 72.9 and 73.5 kJ mol^{-1}, respectively. The similar activation energies reflect that the ionic conduction mechanisms for both $Bi_{17}V_3O_{33}$ and the high-temperature phase are similar. Figure 5 shows the typical impedance plots for the high-temperature phase at 500 and 700 °C. At 500 °C, the grain boundary contribution is clear. As the temperature increases, such as at 700 °C, the grain boundary effect was eliminated. The conductivity at 500 °C is 1.03×10^{-3} $S \cdot cm^{-1}$. An ionic conductivity study of the V_2O_5-doped Bi_2O_3, $(V_2O_5)_{1-x}(Bi_2O_3)_x$, obtained by solid-state reactions, demonstrated that the composition with x=0.14 shows the best ionic conductivity (σ_{500} °C = 2.2×10^{-3} $S \cdot cm^{-1}$).[13] As we discussed above, the hydrothermal route leads to the stoichiometric $Bi_{17}V_3O_{33}$ compositions for both compounds and its high-temperature phase, and both phases also showed comparable high conductivity.

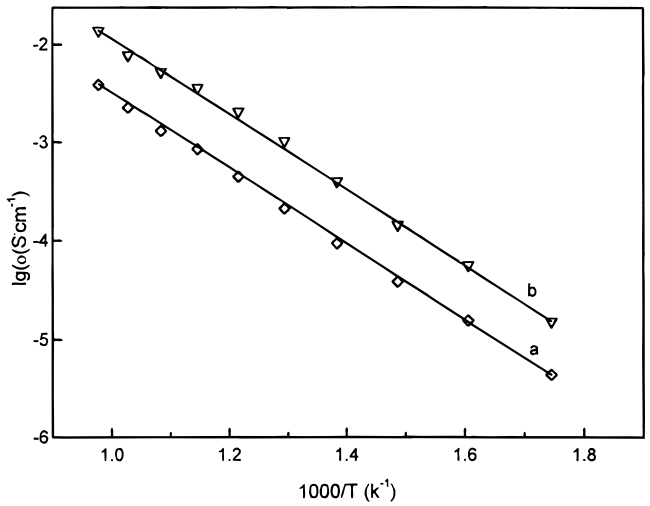

Figure 4. Arrhenius plots of conductivity for the samples sintered at (a) 700 °C and (b) 850 °C.

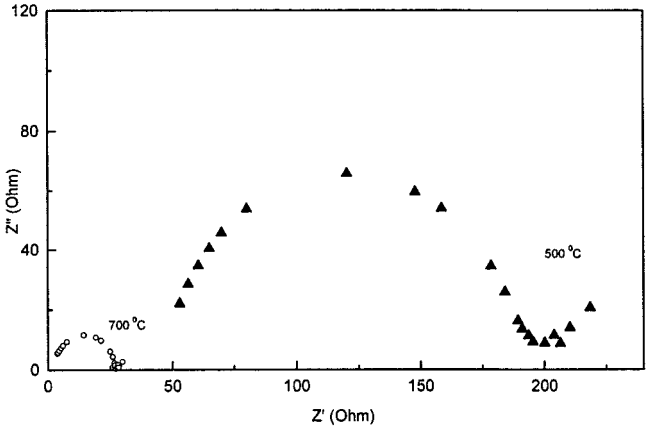

Figure 5. Complex impedance plane diagrams at 500 and 700 °C for the sample sintered at 850 °C.

Conclusions

In summary, a vanadium-stabilized superstructure phase $Bi_{17}V_3O_{33}$ was hydrothermally synthesized. Its structure can be described as a $\sqrt{5} \times \sqrt{5} \times 2$ superlattice structure derived from the fluoride subcell. $Bi_{17}V_3O_{33}$ is a metastable compound and both $Bi_{17}V_3O_{33}$ and its high-temperature phase show comparable high ionic conductivity.

CM9801284

(22) Hardcastle, F. D.; Wachs, I. E.; Eckert, H.; Jefferson, D. A. *J. Solid State Chem.* **1991,** *90,* 194.